Investigation of mass transport processes in a microstructured membrane reactor for the direct synthesis of hydrogen peroxide

Laura L. Trinkies [a,1,*], Andrea Düll [a,1,2], Jinju Zhang [a], Sebastian Urban [b], Benedikt J. Deschner [a], Manfred Kraut [a], Bradley P. Ladewig [a], Andreas Weltin [b], Jochen Kieninger [b], Roland Dittmeyer [a,c]

[a] Institute for Micro Process Engineering (IMVT), Karlsruhe Institute of Technology, 76344 Eggenstein-Leopoldshafen, Germany
[b] Laboratory for Sensors, IMTEK - Department of Microsystems Engineering, University of Freiburg, 79110 Freiburg, Germany
[c] Institute of Catalysis Research and Technology (IKFT), Karlsruhe Institute of Technology, 76344 Eggenstein-Leopoldshafen, Germany

HIGHLIGHTS

- Investigation of mass transport through polymer membrane in multi-phase microreactors.
- Permeances of composite PDMS membrane to H_2/O_2 are determined experimentally.
- De-saturation of liquid reaction media via cross-membrane-transport is observed.
- De-saturation behaviour can be modelled using a solution-diffusion model in MATLAB.

GRAPHICAL ABSTRACT
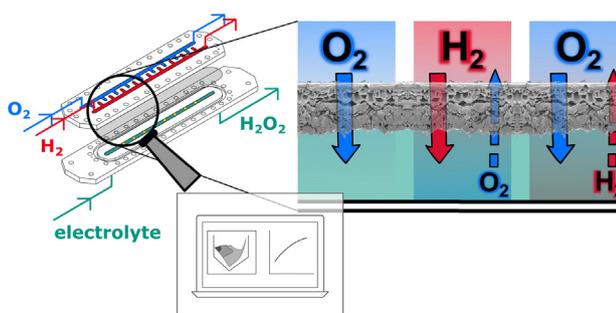
ARTICLE INFO

ABSTRACT

Microstructured membrane reactors present a promising approach to master the productivity and safety challenges during the direct synthesis of hydrogen peroxide. However, various mass transport processes occur in this complex system. In order to gain a deeper understanding of these processes, the saturation and desaturation behaviour of the liquid reaction medium with the gaseous reactants is investigated experimentally to examine possible cross-contamination. Moreover, the employed PDMS membrane's permeances to hydrogen and oxygen are researched at different pressures, by using a variable-pressure/constant-volume setup for the behaviour at ambient pressure and a constant-pressure/variable-volume setup for the behaviour at elevated pressures. A mathematical model in MATLAB is applied to simulate the results. It is shown that a certain desaturation of the gasses through the membrane occurs, and the results are underlined by the modelled ones using a solution-diffusion model in MATLAB. Thus a constant flushing of the gas channels of the reactor is required for safety reasons. Moreover, the measured permeance values indicate that the species transport is mainly limited by the diffusion in the liquid phase and not the membrane resistance.

* Corresponding author.
E-mail addresses: laura.trinkies@kit.edu (L.L. Trinkies), andrea.duell@kit.edu (A. Düll), jinju.zhang2@kit.edu (J. Zhang), sebastian.urban@imtek.de (S. Urban), benedikt.deschner@kit.edu (B.J. Deschner), manfred.kraut@kit.edu (M. Kraut), manfred.kraut@kit.edu (B.P. Kraut), bradley.ladewig@kit.edu (B.P. Ladewig), weltin@imtek.de (A. Weltin), kieninger@imtek.uni-freiburg.de (J. Kieninger), roland.dittmeyer@kit.edu (R. Dittmeyer).
[1] These authors contributed equally to this work.
[2] Current address: Institute for Chemical Technology and Polymer Chemistry (ITCP), 76131 Karlsruhe, Germany.

1. Introduction

Oxidation reactions play an important role in the synthesis of platform chemicals for the manufacturing of various everyday products (Goor et al., 2000; Wilson et al., 2017). While chlorinated oxidizers have found a wide application in these processes, their severe impact on the environment and human health has motivated the search for less hazardous reagents (Ciriminna et al., 2016; Flaherty, 2018). With its only oxidation byproduct being water (H_2O), hydrogen peroxide (H_2O_2) is such a "green" alternative (Campos-Martin et al., 2006; Ciriminna et al., 2016).

Currently, H_2O_2 is mainly synthesized via the antraquinone auto-oxidation (AO) process (Goor et al., 2000), which accounts for more than 95% of the total H_2O_2 production (Yi et al., 2016). However, the AO process has severe drawbacks, like a high energy demand (Campos-Martin et al., 2006) or the generation of gaseous, liquid and solid waste, which negatively affect the sustainability of the process (Yi et al., 2016). Moreover, the production via the AO process is economically feasible only on a large scale due to the process complexity and the numerous required downstream unit operations (Samanta, 2008; Paunovic et al., 2015). The long-distance transport associated with this centralized production of H_2O_2 requires an energy-intensive concentration of the aqueous peroxide solutions up to 70 wt.% H_2O_2, which stands in contrast with typical end-user requirements of dilute solutions with less than 9 wt.% H_2O_2. Moreover, it poses a potential safety hazard (Yang et al., 2018) and increases the chemical's price (Campos-Martin et al., 2006).

Due to the aforementioned drawbacks, the development of small-scale processes suitable for an on-site and on-demand production of H_2O_2 in plants is of great interest (Centi et al., 2009; Paunovic et al., 2015). The direct synthesis from H_2 and O_2 in a microstructured membrane reactor is one of these approaches. In the optimization of the multiphase reactor currently employed by our group for the direct synthesis of H_2O_2 (Selinsek et al., 2016; Selinsek et al., 2018), the reduction of mass transfer resistances plays an important role. On the other hand, it is crucial to ensure process safety under all operating conditions, which means that the accumulation of gaseous H_2, O_2 and their explosive mixtures must be prevented (Centi et al., 2009; García-Serna et al., 2014).

By introducing a membrane as a semipermeable barrier between the liquid channel and the two separate gas channels flushed with either H_2 or O_2, the aqueous reaction medium is intended to be resaturated with the gaseous reactants to increase the product concentration at the reactor outlet while ensuring process safety (Pashkova et al., 2008; Pashkova et al., 2010; Pashkova et al., 2013; Selinsek et al., 2016). A possible concept for this reactor principle is shown in Fig. 1 a). However, as the liquid in contact with the membrane contains both reactants A and B (H_2 and O_2) at the same time while the other side of the membrane is flushed with merely one of the two gases, an opposite driving force exists for the diffusion of dissolved gas A (H_2 or O_2) through the membrane into the gas channel of the respective other gas B (O_2 or H_2, respectively). This is schematically illustrated in Fig. 1 b).

Therefore, the qualitative and quantitative analysis of this undesirable desaturation of the liquid in the membrane microreactor, i.e. gas transport in the opposite direction as intended in the initial reactor concept, is of particular interest. As the occurrence of such cross-contamination entails potential risks to process safety, these investigations have already been deemed important (Selinsek et al., 2016). However, it is crucial to fully understand the mass transfer processes occurring within the system first. This is done by an experimental as well as theoretical investigation of the asymmetric polydimethylsiloxane (PDMS) membrane acting as a gas–liquid contactor in the microreactor for direct synthesis of H_2O_2 to reveal the mass transfer processes.

2. Materials and methods

2.1. Experimental investigation of the occurence of cross-contamination

Because of their capability of real-time monitoring, *in situ* measurement techniques are becoming more and more important in the monitoring processes of flow reactors (Li et al., 2021). This is why also for this work, electrochemical microsensors integrated into the microreactor were developed and applied to gain a deeper insight into the phenomena occurring inside the reactor. The microsensors comprise platinum (Pt) working and counter electrodes embedded with a silver/silver bromide (Ag/AgBr) reference electrode in polymeric plugs to be installed in the reactor. A multistep chronoamperometric sensor protocol allows temporally resolved, local detection of H_2, O_2, and H_2O_2 by measuring the currents caused by the oxidation (H_2, H_2O_2) or reduction (O_2) of the analytes at the working electrodes when applying specific electrode potentials (Urban et al., 2018; Urban et al., 2020; Urban et al., 2021). A schematic representation of the membrane reactor
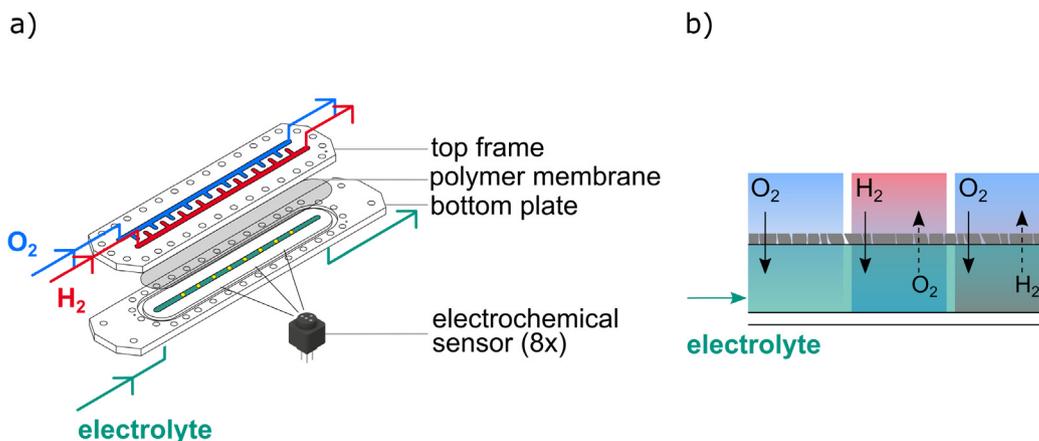

Fig. 1. (a) Schematics of the membrane reactor designed for the direct synthesis of H_2O_2 in a microstructured membrane reactor, adapted from (Urban et al., 2021). (**b**) Schematics of the problem of counter-diffusion.
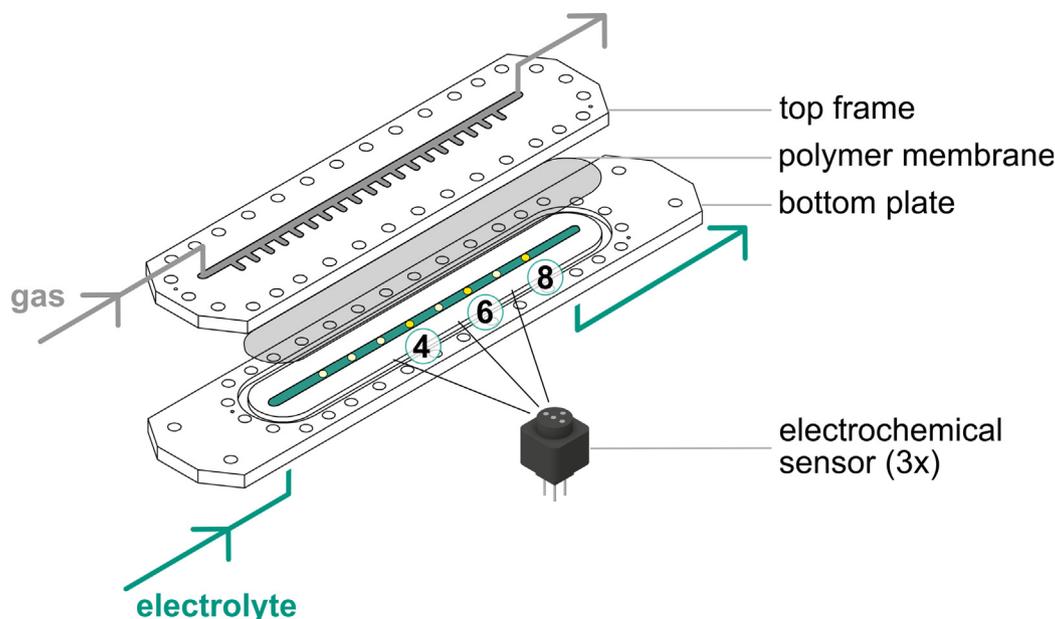
Fig. 2. Schematic representation of the membrane reactor used for the investigation of the (de-) saturation of the aqueous reaction medium with H_2 or O_2.

used for the investigation of the (de-) saturation of the aqueous reaction medium with H_2 or O_2 can be taken from Fig. 2.

The module consists of a top plate containing a long, straight channel with 19 perpendicular side arms (10 mm × 4 mm × 0.8 mm) for the gas flow and a bottom plate containing a 241 mm long, straight channel of a width and depth of 4 mm and 0.5 mm, respectively, for the liquid flow. As a physical barrier between the two phases, a composite membrane is placed between the metal plates with its dense layer oriented towards the liquid medium (more detailed description: see Section 2.2). Several slots at the base of the liquid channel enable the mounting of the electrochemical sensors at variable positions along the channel length. The plugs are held in place by a metal frame screwed onto the back of the bottom plate. In the experiments presented hereafter, three sensors are installed at positions ④, ⑥ and ⑧, as indicated in Fig. 2, while epoxy plugs are used to seal the other openings.

The aqueous reaction medium (H_2O + 0.15 mmol/l H_2SO_4 + 4 mmol/l NaBr) contained in a glass bottle placed on a magnetic

stirrer (VMS-C7 Advanced, VWR) is saturated with a pure gas or a gas mixture, which is dosed with the help of two rotameters (DK800/N and DK800/PV, KROHNE). The saturated liquid is then fed into the reactor via a micro annular gear pump (mzr-7205, HNP Mikrosysteme), while the gas flow through the opposite reactor channel, which is separated from the liquid side by a membrane, is set by a mass flow controller (EL-FLOW Select, Bronkhorst). Upon exiting the reactor, the liquid is led into a residual container positioned on a balance (CP 8201, Sartorius). The experimental setup is shown in Fig. 3.

To relate the electrochemical sensors' output signal to the corresponding concentrations of dissolved O_2 or H_2, the sensors mounted in the assembled membrane reactor are first calibrated by saturating the aqueous reaction medium with H_2/N_2 or O_2/N_2 gas mixtures of defined compositions before feeding it to the reactor at a flow rate of 1.2 ml min^{-1}. An identical gas mixture is fed to the gas side of the reactor, thereby preventing any changes in dissolved gas concentration due to transmembrane gas transport.
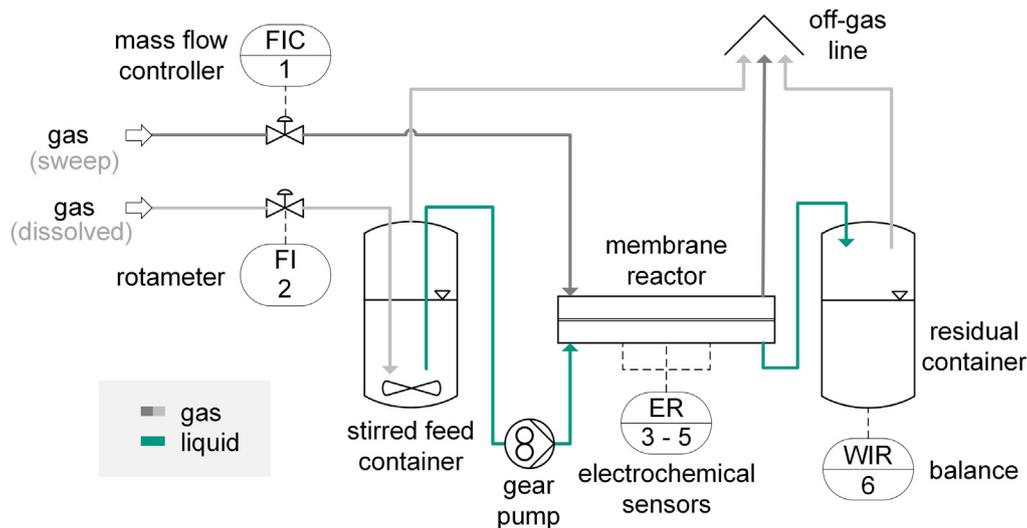

Fig. 3. Process flow diagram visualizing the experimental setup for the determination of dissolved gas concentration profiles during (de-) saturation in the membrane reactor.

Table 1
Overview of the conducted experiments concerning the (de-) saturation of the aqueous reaction medium in the membrane reactor: type of gas used for the liquid's saturation before the reactor inlet, type of gas used for sweeping the opposite reactor side, as well as measured liquid flow rates, corresponding residence times and sweep gas flow rates.

Name	$Gas_{dissolved}$	Gas_{sweep}	$\dot{V}_L$	τ_L	$\dot{V}_{G,sweep}$
-	-	-	ml min^{-1}	s	ml min^{-1}
SH	N_2	H_2	1.15	25.2	349
SO	N_2	O_2	1.24	23.3	266
DH	H_2	N_2	1.23	23.5	271
DO	O_2	N_2	1.18	24.5	327

Fig. 5. Process flow diagram visualizing the experimental setup for the determination of membrane permeances at ambient pressure; sample gas either H_2 or O_2.

The data points collected for the sensor calibration along with the determined, linear calibration curves are presented in Figs. A1 and A2 in the Supplementary Information. All experiments are carried out in the absence of a catalyst at an absolute pressure of 1.01 bar with negligible differential pressure across the membrane and a temperature of 298.15 K. In all experiments discussed hereafter, the pump's liquid flow rate is set to 1.2 ml min^{-1}. An overview of the conducted experiments to determine a potential cross-contamination is given in Table 1 along with the measured gas and liquid flow rates $\dot{V}$.

The actual experiments are separated into two parts. Firstly, local concentration measurements are conducted during the saturation of the unsaturated liquid with either H_2 or O_2 to obtain reference data points. Secondly, concentration profiles are determined during the desaturation of the reaction medium, which is initially saturated with H_2 or O_2 while the gas channel is swept with N_2. Thus, in this study, N_2 is used to replace either H_2 or O_2 for safety reasons, while in the actual reactor, a binary H_2/O_2 gas mixture would be present.

2.2. Impact of membrane resistance on the overall species transport

In order to evaluate the influence of the membrane on the species transport from the gas phase into the liquid phase (or vice versa), its permeance to the reactants H_2 and O_2 needs to be determined.

The membrane envisaged for further use in the new reactor concept is a 204 μm thick composite polymer membrane (PDMS flat sheet membrane, PERVATECH BV). As shown in Fig. 4 it consists of a dense, hydrophobic polydimethylsiloxane film with pore sizes much smaller than 4 μm, which is deposited onto a porous polyimide (PI) intermediate layer and a porous polyethylene terephthalate (PET) support layer.
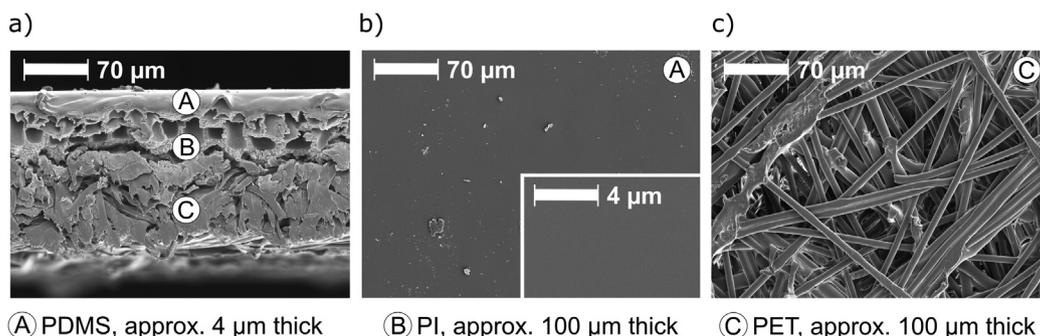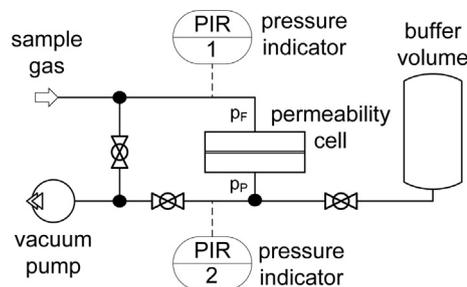
2.2.1. Experimental determination of membrane permeances at ambient pressure

The membrane permeances are determined by employing the variable pressure/constant volume setup presented in Fig. 5. The permeance test cell consists of two metal frames. A 47 mm wide membrane sample is placed into the lower frame onto a metal support grid. The cell is then sealed by placing an O-ring with an inner diameter of 40 mm on top of the membrane and mounting the upper frame.

During the experimental trials, the experimental setup is divided into a high-pressure and a low-pressure section by using ball valves. While the former is connected to the sample gas bottle via a pressure regulator, the latter is connected to a buffer container with a volume of 250 ml. A vacuum pump (E2M0.7, EDWARDS) is installed to evacuate the system down to approximately 0.02 mbar and two pressure transmitters (S-20, WIKA) indicate the absolute upstream and downstream system pressures.

For each species, the upstream (high-pressure) side is flooded with sample gas, the vacuum pump is switched off once the downstream (low-pressure) side is fully evacuated and the absolute pressures are monitored and recorded on either side of the membrane. The experiments are carried out at a temperature of 298.15 K and an average upstream pressure of 1.57 and 1.23 bar for the sample gasses H_2 and O_2 respectively.

The permeance values $\mathscr{P}$ are determined from the temporal evolution of the negative logarithm of the difference between upstream and downstream pressures. As can be derived from a material balance over the system's downstream section under the assumption of the validity of the ideal gas law and the simple solution-diffusion model, this follows a linear relationship according to Eq. (1). In the equation, the feed and permeate pressures are denoted by p_F and p_P respectively. Moreover, A represents the membrane area, R the ideal gas constant, T the system temperature, V the downstream volume and t represents the elapsed time.

Fig. 4. SEM pictures: (**a**) membrane cross section, (**b**) top view of the upper selective PDMS-layer Ⓐ and (**c**) top view of the lower PET-support layer Ⓒ.
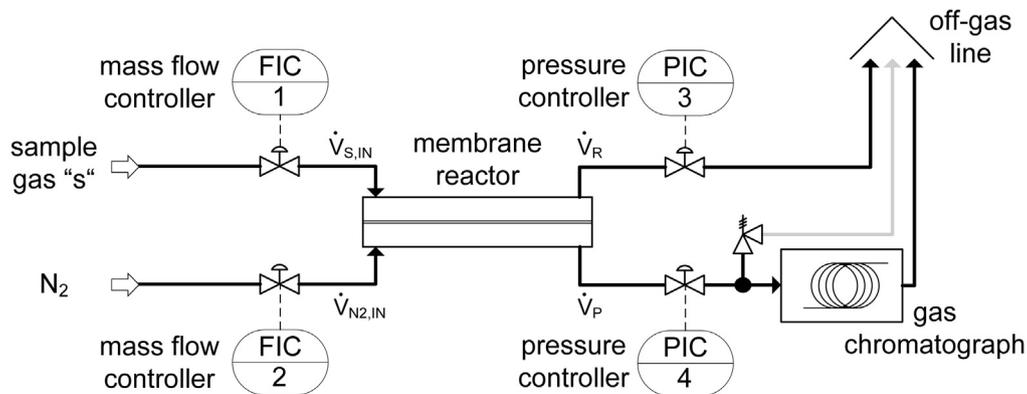
Fig. 6. Process flow diagram visualizing the experimental setup for the investigation of the influence of absolute pressure on the membrane permeance; sample gas either H_2 or O_2.

$$-\ln\left(\frac{p_F - p_P}{p_F^{t=0} - p_P^{t=0}}\right) = \underbrace{\mathscr{P}A\frac{RT}{V}}_{\text{slope}}t \qquad (1)$$

2.2.2. Experimental determination of membrane permeances at elevated pressures

A constant-pressure/variable-volume setup is employed to also determine the influence of the absolute pressure on the membrane permeance, as visualized in Fig. 6. This is relevant because the membrane reactor for the direct synthesis of H_2O_2 is sought to be operated at elevated pressures up to 100 bar to increase the concentration of the gaseous reactants in the liquid solvent and hence increase the product concentration (Selinsek et al., 2018). To determine the membrane transport properties without the influence of the transport resistance in the liquid boundary layer, the reactor's liquid channel is swept with an inert gas instead of being flushed with the aqueous reaction medium.

The sample gasses H_2 and O_2 and the inert gas N_2 are fed to the membrane reactor shown in Fig. 6 via two mass flow controllers (EL-FLOW Select, Bronkhorst). In order to determine its composition, the permeate stream is led to a gas chromatograph (8860 GC System, Agilent) via a pressure relief valve to set the maximum pressure at the instrument's inlet. Calibration curves determined for the GC with H_2 or O_2 and N_2 as internal standard can be found in Fig. A3 in the Supplementary Information. The system pressure on either side of the membrane is set by a pressure controller (EL-PRESS, Bronkhorst).

Before each experiment, the membrane reactor is thoroughly flushed with sample gas and checked for leakages by monitoring the system's pressure loss occurring over a time range of approximately ten minutes when not being swept with sample or inert gas. In case of an acceptable leak rate, the sample gas MFC is adjusted to a set point of 100% and the inert gas flow rate is set to approximately 81.6 ml min^{-1}.

Once the permeate composition quasi-continuously monitored by the gas chromatograph (GC) reaches a constant value, retentate samples are taken with a gas collection tube and individually injected into the GC. Additionally, permeate and retentate flow rates are determined with the help of a gas flow calibrator (Definer 220, DryCal).

Separate series of experiments with individual membrane samples are conducted for the sample gasses H_2 and O_2 at an ambient temperature of 298.15 K and pressures of 15 bar, 20 bar and 25 bar applied to both sides of the reactor. Additional experiments are carried out at ambient pressure (1.01 bar) by taking permeate and retentate samples at the reactor outlet with the help of the gas collection tube as direct feeding of the permeate stream to the GC wasn't realizable at such a low system pressure due to the high pressure drop in the connection line.

2.3. Modelling

To check, whether the membrane permeances determined with the variable-pressure/constant-volume method at ambient pressure are valid at elevated pressure levels, a mathematical model of the membrane reactor as schematically visualized in Fig. 7 is employed.

A simplified one-dimensional model has been developed to describe mass transport of up to four components ($i = 1, \ldots, 4$) between a gaseous and a liquid phase. The phases are separated by an asymmetric membrane consisting of a porous and a dense membrane layer. The system is considered to be isobaric and isothermal, and the gas behaviour is assumed to be ideal.
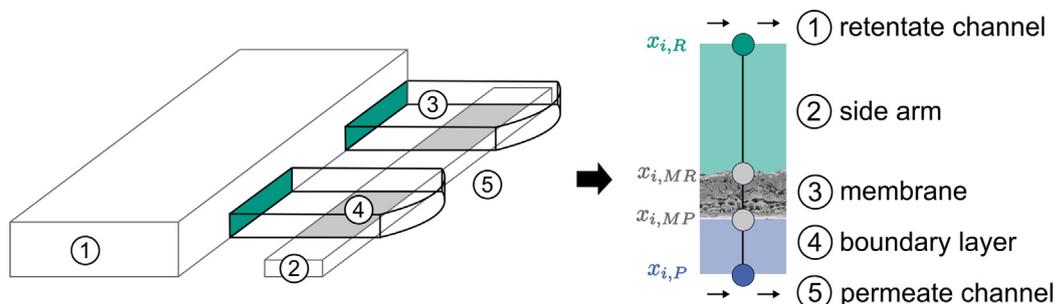

Fig. 7. Schematic visualization of the simplified MATLAB model employed to evaluate the experimental results.
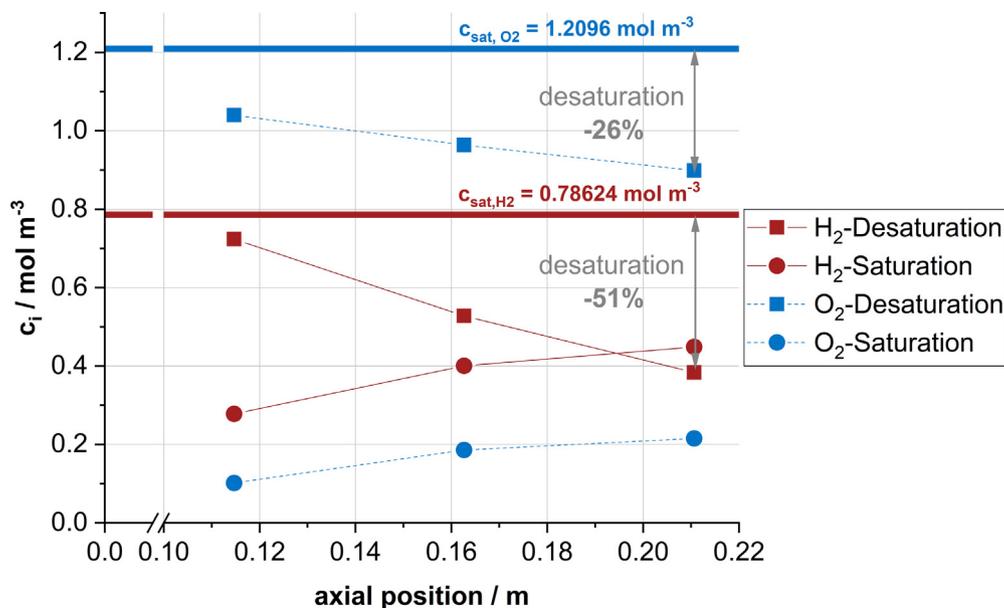
Fig. 8. H_2 and O_2 concentrations determined during saturation and desaturation experiments at sensor positions 4, 6 and 8 in the liquid flow channel; H_2 and O_2 saturation concentrations $c_{sat,i}$ marked by a thick line, calculated by Henrys Law. Lines are added to guide the eye and do not represent measured data points.

Mass transport through dense membranes is a purely diffusive process (Nagy, 2012), however, controlled by the thermal motion of the polymer molecules making up the membrane matrix (Yampolskii et al., 2006). The most widely used model to describe this phenomenon, which is also used in the model implemented in this study, is the solution-diffusion model (SDM) (Yampolskii et al., 2006).

In the model, evaluated in MATLAB, the 19 membrane patches of the reactor described in Fig. 2 are considered sequentially. Starting from the inlet, the sample and inert gas transmembrane flows are iteratively determined based on the known gas compositions in the two gas channels by taking into account the non-equimolar counterdiffusion in the side arm as described by Eq. (2), the species transport through the membrane as described by Eq. (3) and the diffusion through the concentration boundary layer at the membrane's permeate side as described by Eq. (4), with the mole flux $\dot{N}_i$ for species i, the areas A of the channel and the membrane, noted by the corresponding subscript, the pressure p, the ideal gas constant R, the operating temperature T, the binary diffusion coefficient D_i for gas i, the thickness of the channel δ_{ch}, the mole fractions x_i of the retentate and permeate, the permeability P_i and the mass transfer coefficient β_i.

$$\dot{N}_i = A_{ch}\frac{p}{RT}\dot{r}_i\frac{D_i}{\delta_{ch}}\ln\left(\frac{\dot{r}_i - x_{i,R}}{\dot{r}_i - x_{i,MR}}\right) \quad \text{with} \quad \dot{r}_i = \frac{\dot{N}_i}{\sum\dot{N}_i} \quad (2)$$

$$\dot{N}_i = A_{mem}\mathscr{P}_i p(x_{i,MR} - x_{i,MP}) \quad \text{with} \quad A_{mem} \neq A_{ch} \quad (3)$$

$$\dot{N}_i = A_{mem}\frac{\beta_i}{RT}p(x_{i,MP} - x_{i,P}) \quad (4)$$

The new gas compositions, which serve as the known boundary values at the following membrane patch, are then determined from species balances applied to the retentate and permeate gas channels.

The binary diffusion coefficients are estimated with the Fuller equation (Fuller et al., 1966) according to Eq. (5) using the molar masses M and diffusion volumes V:

$$D_{1,2} = \frac{10^{-3}T^{1.75}\left(\frac{1}{M_1} + \frac{1}{M_2}\right)^{0.5}}{p\left[\left(\sum_i V_{i1}\right)^{\frac{1}{3}} + \left(\sum_i V_{i2}\right)^{\frac{1}{3}}\right]^2} \quad (5)$$

3. Results

3.1. Investigation of the occurence of cross-contamination

The concentrations determined with the help of the electro-chemical sensors at sensor positions ④, ⑥ and ⑧ along the length of the membrane reactor's liquid channel are presented in Fig. 8 for the desaturation and saturation of the aqueous reaction medium with H_2 and O_2. The liquid measured at position ④ has passed eight resaturation patches, the one at position ⑥ twelve and the one at position ⑧ sixteen. All obtained concentration profiles follow the expected trend of decreasing concentrations during desaturation and increasing concentrations during saturation with increased distance from the channel inlet. H_2 transmembrane flows exceed the corresponding O_2 transmembrane flows, which is mainly attributed to the component's higher diffusivity in the liquid phase, while the membrane's slightly higher permeance to H_2 is expected to play an additional but minor role. The concentration of dissolved H_2 (O_2) measured at the sensor positioned closest to the channel outlet (sensor 8, Fig. 2) is decreased by 51% (26%) compared to the fully saturated liquid entering the system during the desaturation experiments while the saturation is increased to 57% (18%) compared to the unsaturated liquid during the reference saturation experiments. It can thus be concluded that the transmembrane H_2 and O_2 flows during saturation and desaturation processes are in the same order of magnitude.

This finding is of crucial importance for the optimization of the membrane reactor design as it suggests the possibility for a counterproductive application of membrane contactors, namely when liquid highly saturated with both reactants comes into contact with an H_2 (O_2) membrane patch and the undesirable desaturation
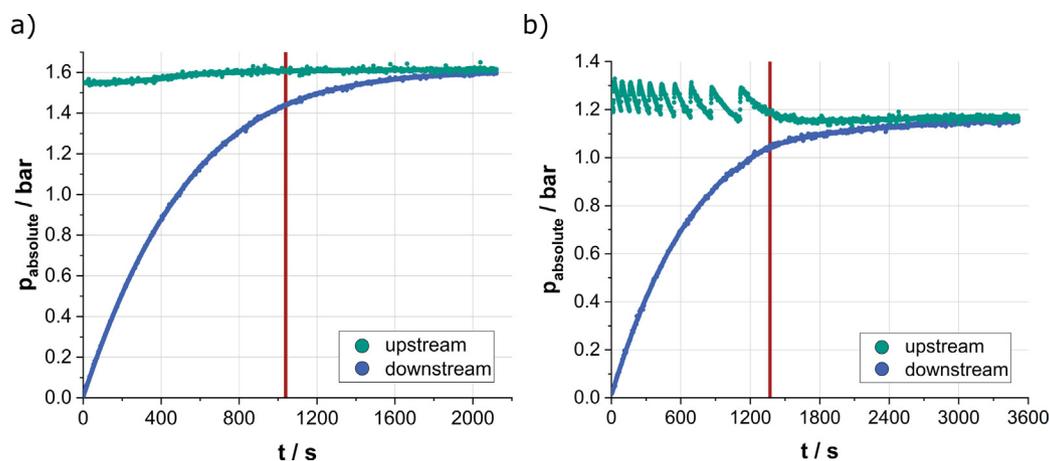
Fig. 9. Temporal evolution of up- and downstream pressure during permeance experiments with sample gasses (**a**) H_2 or (**b**) O_2; time limit until which the data is considered for evaluation marked by a red line.
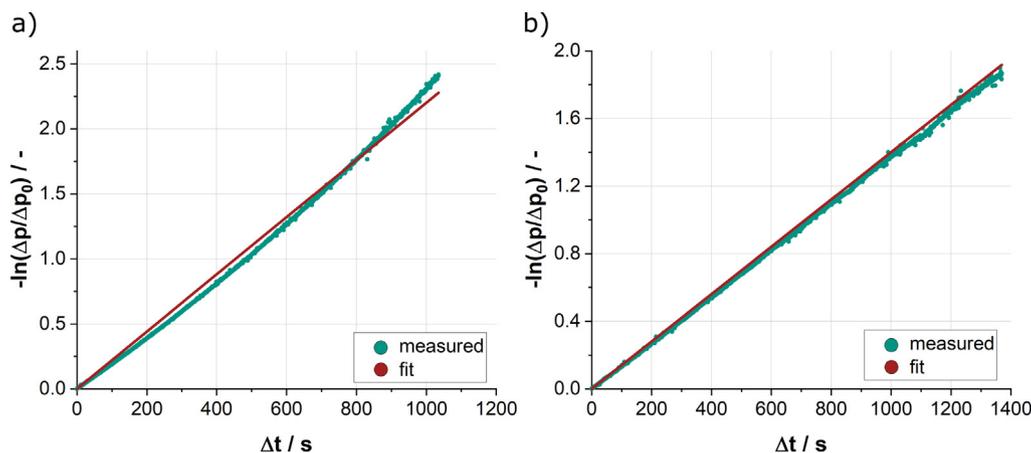

Fig. 10. Temporal evolution of the negative logarithm of the differential pressure relative to the initial pressure difference determined from permeance experiments with sample gasses (**a**) H_2 or (**b**) O_2; line fitted to the experimental data points (green) according to Eq. (1) indicated in red.

Table 2
Slope and R^2 of the lines fitted to the experimental data points along with the calculated membrane permeances $\mathscr{P}$ and approximate PDMS permeabilities P.

Gas	Slope	R^2	$\mathscr{P}_{Membrane}$	P_{PDMS}
–	s^{-1}	–	mol m^{-2} Pa^{-1} s^{-1}	mol m^{-1} Pa^{-1} s^{-1}
H_2	0.0022	0.998	$1.77 \cdot 10^{-7}$	$7.06 \cdot 10^{-13}$
O_2	0.0014	1.00	$1.12 \cdot 10^{-7}$	$4.49 \cdot 10^{-13}$

with O_2 (H_2) at this patch outweighs the intended saturation with O_2 (H_2) at an O_2 (H_2) membrane patch.

3.2. Impact of membrane resistance on the overall species transport

3.2.1. Determination of membrane permeances at ambient pressure

The recorded data visualized in Fig. 9 a) and b) for H_2 and O_2 respectively shows the expected logarithmic growth of the downstream pressure until the pressure difference between the two sides of the permeation cell approaches zero following the procedure described in the methods. Strong oscillations are detected in

the upstream O_2 pressure, which is most likely due to a malfunctioning O_2 pressure regulator used in the experiments. A loose spring inside the regulator might have caused the vibrations in consequence of the flowing fluid. For compensation of this effect, an averaged upstream pressure is considered for the evaluation.

The permeance then can be calculated from the slope of the fitted line. Data is considered until the time when the ratio between down- and upstream pressure exceeds 90% as marked in Fig. 9 by vertical red lines due to increased data scattering at differential pressures approaching zero. As can be taken from Fig. 10 a) and b) for the sample gasses H_2 and O_2 respectively, the experimental

Table 3

Constant-pressure/variable-volume method: sample gas s, absolute system pressure p, as well as measured outlet flow rates $\dot{V}_i$ at SATP, mole fraction of sample gas in the permeate stream $x_{S,P}$ and mole fraction of inert gas in the retentate stream $x_{N_2,R}$. The inlet flows for O_2 and H_2 as well as N_2 were kept constant at 267 ml min^{-1}, 346 ml min^{-1} and 82 ml min^{-1} respectively.

Index	Sample	$\mathbf{p}$	$\dot{V}_P$	$\dot{V}_R$	$x_{S,P}$	$\mathbf{x}_{N_2,R}$
-	-	bar	ml min^{-1}	ml min^{-1}	%	%
H1	H$_2$	1.01	89.5	337.1	14.5	2.5
H2	H$_2$	15.00	106.1	319.9	41.9	6.4
H3	H$_2$	20.00	107.2	321.9	44.6	7.0
H4	H$_2$	25.00	107.2	323.0	47.1	7.6
O1	O$_2$	1.01	85.8	260.4	7.8	1.6
O2	O$_2$	15.00	88.4	255.1	18.4	3.8
O3	O$_2$	20.00	88.3	263.4	19.5	4.2
O4	O$_2$	25.00	87.6	261.1	21.1	4.4

data is in good agreement with this theoretical consideration. The slopes of the fitted lines along with the corresponding R^2 as a measure of confidentiality can be taken from Table 2. Furthermore, the calculated permeances of the composite membrane and the approximate PDMS permeabilities estimated as the ratio between the overall membrane permeance and the thickness of the dense PDMS layer (4 μm) are listed. The latter are to be used to evaluate the reliability of the experimental data.

The determined PDMS permeabilities lie in the same range as published data (Hägg, 2000; Merkel et al., 2000) with the obtained absolute values slightly exceeding the reported permeabilities. This is most likely to be attributed to a different layer structure as permeabilities are strongly dependent on the specific degree of polymer cross-linking and the curing procedure (Hägg, 2000). The membrane is found to be slightly more permeable to H$_2$ than to O$_2$, which is consistent with findings presented in literature and can be attributed to the fast diffusion of H$_2$ in PDMS due to its small molecular size (Merkel et al., 2000).

As in the real membrane reactor, one membrane side is intended to be swept with a pure gas while the other one is in contact with a liquid phase. Thus, the total resistance to H$_2$ and O$_2$ species transport can be described as the sum of the experimentally determined membrane transport resistance and the resistance imposed by the liquid phase as visualized in Fig. 7 and formulated in Eq. (A1) where $\dot{N}$ is the transferred mole flow, H represents the Henry constant and β is the mass transfer coefficient.

$$\dot{N}_i = A \frac{1}{\underbrace{\dfrac{H_i}{\mathscr{P}_i}}_{\text{membrane}} + \underbrace{\dfrac{1}{\beta_i}}_{\text{liquid}}} \left(p_{i,G} H_i - c_{i,L} \right) \qquad (6)$$

In order to compare the individual contributions, the transport resistance imposed by the liquid phase is determined from mass transfer coefficients roughly estimated with the help of a Sherwood correlation (VDI-Wärmeatlas, 2013) under the assumption of a developed hydrodynamic and concentration boundary layer to $1.96 \cdot 10^{-5}$ m/s and $1.25 \cdot 10^{-5}$ m/s for the diffusing species H$_2$ and O$_2$ respectively. It can be concluded that in the present system, species transport is governed by the diffusion in the liquid phase with the membrane resistance merely making up 0.09% (H$_2$)/0.13% (O$_2$) of the total transport resistance.

3.2.2. Determination of membrane permeances at elevated pressures

All conducted experiments are listed in Table 3 along with the permeate and retentate volume flow rates measured at the reactor's inlet or outlet at Standard Ambient Temperature and Pressure (SATP). The corresponding leak rates are given in Table A1 in the Supplementary Materials. For the sake of clarity, the individual gas streams are indicated in Fig. 6. The corresponding permeate and retentate composition in terms of the mole fraction x_i, the

Table 4

Outlet compositions obtained with a simplified system model along with the transmembrane species flows and discrepancies between model (m) and experiment (e).

Index	$x_{S,P}$	$x_{N_2,R}$	$\Delta\dot{V}_{S,P}^{(m-e)}$	$\Delta\dot{V}_{N_2,P}^{(m-e)}$
-	%	%	ml min^{-1}	ml min^{-1}
H1	8.4	1.0	5.7	5.1
H2	41.1	6.3	1.5	0.2
H3	44.2	6.9	1.0	0.4
H4	46.2	7.4	1.0	1.2
O1	4.9	1.1	2.6	1.2
O2	17.8	4.3	1.1	1.7
O3	18.6	4.5	1.3	0.9
O4	19.1	4.7	2.1	0.7

transmembrane flows, as well as the absolute and relative species imbalances, based on the sample or inert gas inlet volume flow $\Delta\dot{V}_i/\dot{V}_{i,IN}$, are given in Table A2.

Though gas leakage is observed in all cases, the corresponding leak rates are relatively low as can be taken from Table A1. Its influence on the experimental results is therefore assumed to be negligible.

While the relative species imbalances, i.e. the relative errors of individual species balances applied on the overall system, are well below 5%, the correpsonding absolute values lie in the same range as the transmembrane flows in case of the experiments conducted at ambient pressure (indices O1 and H1). Data collected in these experiments is therefore expected to be less accurate than values obtained from experiments in which the transmembrane flows are considerably higher than the calculated error as it is especially the case with experiments carried out at elevated pressures with H$_2$ as sample gas (indices H2, H3 and H4).

At all pressure levels, H$_2$ transmembrane flows are found to slightly exceed the corresponding O$_2$ quantities, which is consistent with the finding that the membrane is slightly more permeable to H$_2$ and is also attributed to the gas's higher diffusivity in a binary gas mixture with N$_2$.

3.2.3. Comparison with modelled results

The determined permeate and retentate compositions at the reactor outlet are listed in Table 4 and visualized in Fig. 11 in comparison with the experimentally determined compositions. The corresponding deviations between the values obtained with the simplified model and determined in the experiments can also be taken from Table 4. The calculated transmembrane species flows are given in Table A3 in the Supplementary Materials.

While modeled and experimentally determined values are in acceptable agreement for both gases at elevated pressures, relatively high deviations are found at ambient pressure, which is
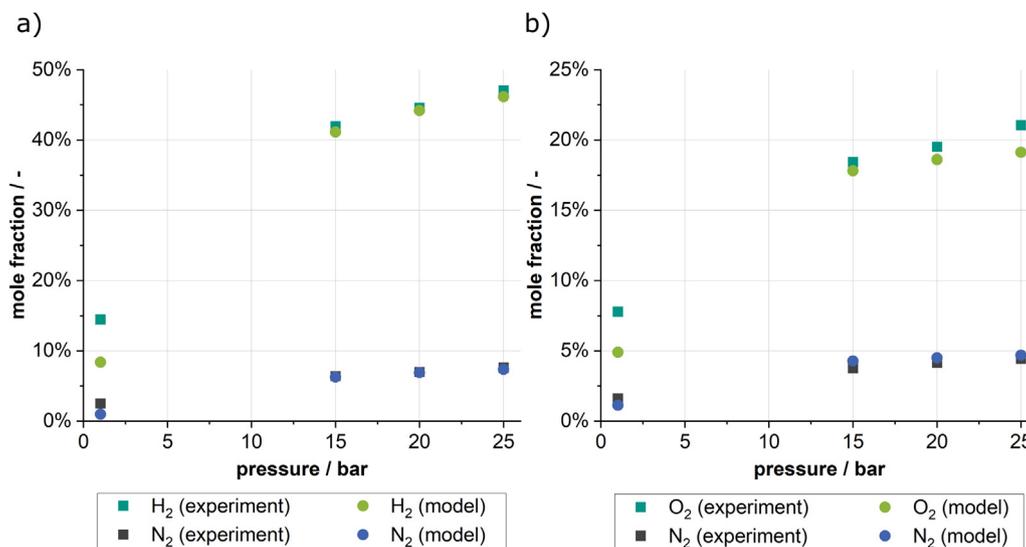
Fig. 11. Comparison between experimentally determined and modeled permeate and retentate outlet composition for both sample gasses (**a**) H_2 or (**b**) O_2.

attributed to the increased experimental inaccuracies due to the species balance errors lying in the same range as the transferred species flows.

As the deviations between modeled and experimentally determined transmembrane flows lie in the same range as the species balance errors for both sample gasses at all four pressure levels investigated, it can be concluded that within the range of the experimental accuracy, the membrane's permeance to H_2 and O_2 is independent of the absolute system pressure up to 25 bar. This is consistent with pressure independent PDMS permeabilities presented in literature, see e.g. (Merkel et al., 2000) or (Shoghl et al., 2017).

It can thus be concluded, that the permeance values determined with the variable-pressure/constant-volume method correctly describe the membrane transport properties at elevated pressures up to at least 25 bar.

4. Discussion

The cross-contamination observed underlines the importance of employing a reactor design in which the gas channels are flushed with H_2 (O_2) to maintain process safety by avoiding the accumulation of O_2 (H_2) in regions with limited convection. However, such "dead zones" exist in the reactor used for the experiments presented in this work due to the side arms connected to the main gas channel as well as in the reactor presented in (Selinsek et al., 2016; Selinsek et al., 2018; Urban et al., 2021).

These observations indicate a possible enhancement of the current reactor design, by employing two different membranes permeable to either H_2 or O_2 but not to both species at the same time. However, non-H_2-permeable membranes are technically still difficult to design for applications at room temperature. The exact membrane permeances in general are expected to be of subordinate importance as the mass transport is highly dominated by the transport resistance in the liquid reaction medium.

Supplementary Materials

The following are available online at https://doi.org/10.1016/j.ces.2021.117145, Figure S1: H_2 calibration curves of the electrochemical sensors., Figure S2: O_2 calibration curves of the electrochemical sensors., Figure S3: H_2 and O_2 calibration curves of the GC., Table S1: Constant-pressure/variable-volume method: sample gas s, absolute system pressure p, leak rate $\triangle p/\triangle t$ as well as detailed measured inlet flow rates $\dot{V}_{i,IN}$., Table S2: Constant-pressure/variable-volume method: mole fraction of sample gas in the permeate stream $x_{S,P}$, mole fraction of inert gas in the retentate stream $x_{N_2, R}$, sample and inert gas transmembrane volume flows $\dot{V}_i$ as well as sample and inert gas absolute and relative imbalances $\triangle \dot{V}_i$., Table S3: Transmembrane species flows obtained with a simplified system model.

Author Contributions

Conceptualization, L.L.T.; methodology, L.L.T., A.D., J.Z, S.U., M.K., A.W., J.K.; software, A.D.; validation, A.D.; formal analysis, A.D.; investigation, L.L.T., A.D.; resources, J.Z., S.U., B.P.L., A.W.; data curation, L.L.T., A.D.; writing—original draft preparation, L.L.T.; writing—review and editing, A.D., J.Z., B.J.D., M.K., B.P.L., A.W., J.K., R.D.; visualization, L.L.T., A.D.; supervision, L.L.T., B.J.D., M.K., J.K.; project administration, L.L.T.; funding acquisition, R.D., All authors have read and agreed to the published version of the manuscript.

Funding

Abbreviations

The following abbreviations are used in this manuscript:

Ag/AgBr	Silver/Silver Bromide
AO	Antraquinone Auto-Oxidation Process
GC	Gas Chromatograph
PDMS	Polydimethylsiloxane
PET	Polyethylene Terephthalate
PI	Polyimide
Pt	Platinum
SDM	Solution-Diffusion Model
SEM	Scanning Electron Microscopy
SATP	Standard Ambient Temperature and Pressure (298.15 K, 1.013 bar)

Symbols

A	area	m^2
β	mass transfer coefficient	$m\,s^{-1}$
c	molar concentration	$mol\,m^{-3}$
δ	thickness	m
D	binary diffusion coefficient	$m^2\,s^{-1}$
H	Henry's law constant	$mol\,m^{-3}\,Pa^{-1}$
M	molar mass	$kg\,mol^{-1}$
$\dot{N}_i$	mole flow	$mol\,s^{-1}$
p	pressure	Pa
P	permeability of the dense membrane	$mol\,m^{-1}\,Pa^{-1}\,s^{-1}$
$\mathscr{P}$	permeance of the composite membrane	$mol\,m^{-2}\,Pa^{-1}\,s^{-1}$
R	ideal gas constant	$8.315\,J\,mol^{-1}\,K^{-1}$
t	time	s
T	temperature	K
V	volume	m^3
x_i	mole fractions	-

Declaration of Competing Interest

The authors declare that they have no known competing financial interests or personal relationships that could have appeared to influence the work reported in this paper

Appendix A. Calibration of the electrochemical sensors

The composition of the liquid phases are calculated using Henry's law with the molar concentration c, Henry's law constant H and the pressure p. The Henry's law constants H for the used
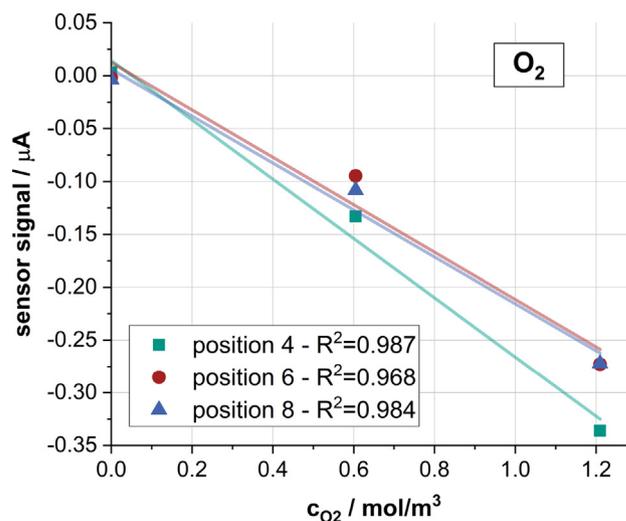

Fig. A1. O_2 calibration curves of the electrochemical sensors mounted in positions 4, 6 and 8.
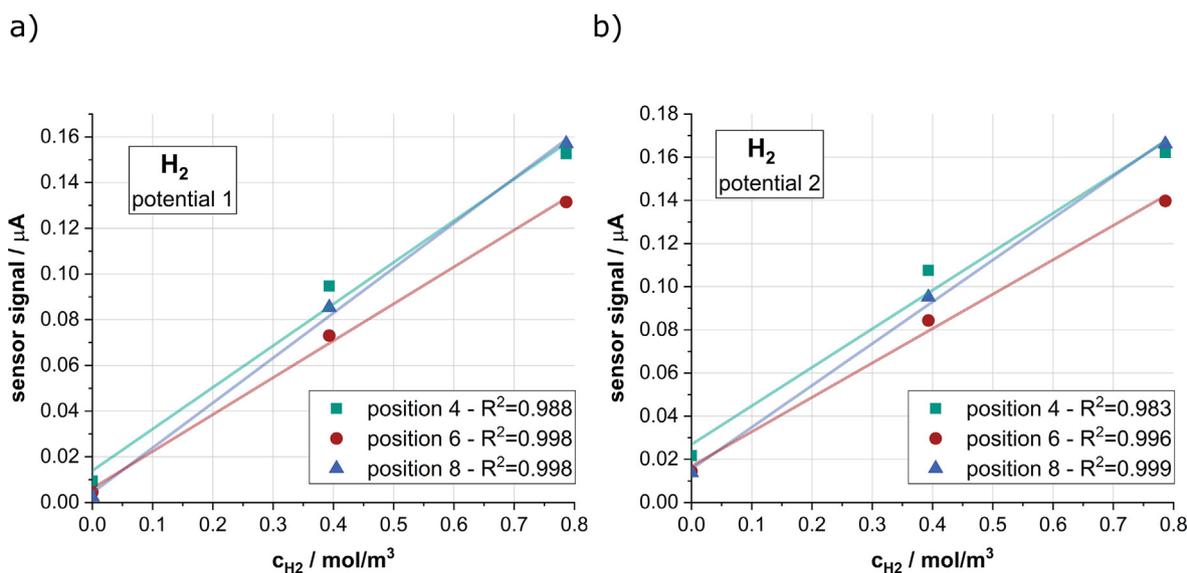
a)

b)

Fig. A2. H_2 calibration curves of the electrochemical sensors mounted in positions 4, 6 and 8 for two different potentials, (**a**) and (**b**).

gasses are widely known and haven been taken from (Sander, 2015).

See Figs. A1 and A2.

$$c = H \cdot p \qquad\qquad (A1)$$

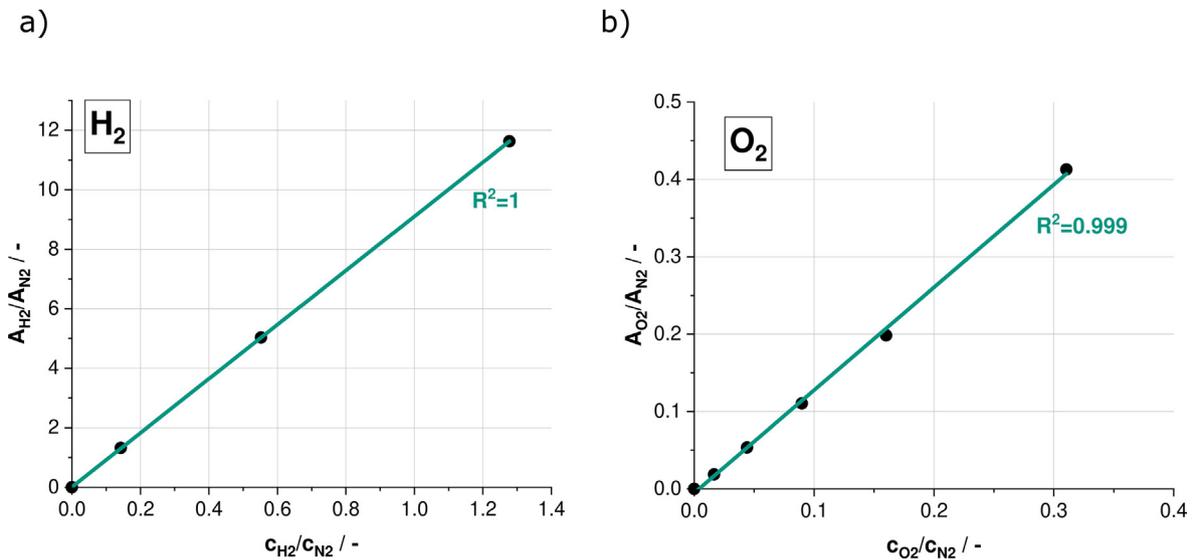## Appendix B. Calibration of the gas chromatograph

See Fig. A3.

Fig. A3. H_2 (**a**) and O_2 (**b**) calibration curves of the GC.

Appendix C. Constant-pressure/variable-volume method: experimental details

See Table A1 and A2.

Appendix D. Modelling results

See Table A3.

Table A1
Constant-pressure/variable-volume method: sample gas s, absolute system pressure p, leak rate $\triangle p/\triangle t$ as well as detailed measured inlet flow rates $\dot{V}_{i,IN}$.

Index	Sample	p	$\Delta p/\Delta t$	$\dot{V}_{S,IN}$	$\dot{V}_{N_2,IN}$
-	-	bar	bar/min	ml min^{-1}	ml min^{-1}
H1	H_2	1.01	-	348.6	81.8
H2	H_2	15.00	0.013	345.8	81.9
H3	H_2	20.00	0.018	345.9	81.4
H4	H_2	25.00	0.027	344.2	81.1
O1	O_2	1.01	-	266.2	81.9
O2	O_2	15.00	0.010	267.6	81.6
O3	O_2	20.00	0.018	267.1	81.6
O4	O_2	25.00	0.018	265.5	81.6

Table A2
Constant-pressure/variable-volume method: mole fraction of sample gas in the permeate stream $x_{S,P}$, mole fraction of inert gas in the retentate stream $x_{N_2,R}$, sample and inert gas transmembrane volume flows $\dot{V}_i$ as well as sample and inert gas absolute and relative imbalances $\triangle \dot{V}_i$.

Index	$\dot{V}_{S,P}$	$\dot{V}_{N_2,R}$	$\Delta \dot{V}_S$	$\Delta \dot{V}_{N_2}$	$\Delta \dot{V}_{S,rel}$	$\Delta \dot{V}_{N_2,rel}$
-	ml min^{-1}	ml min^{-1}	ml min^{-1}	ml min^{-1}	%	%
H1	12.9	8.5	6.9	−3.1	2.0	−3.8
H2	44.5	20.5	1.9	−0.2	0.5	−0.3
H3	47.8	22.6	−1.3	−0.6	−0.4	−0.7
H4	50.5	24.6	−4.7	−0.2	−1.4	−0.3
O1	6.7	4.2	3.2	−1.4	1.2	−1.7
O2	16.3	9.6	5.8	−0.1	2.2	−0.2
O3	17.2	10.9	−2.5	−0.4	−1.0	−0.5
O4	18.5	11.6	−2.5	0.8	−0.9	1.0

Table A3
Transmembrane species flows obtained with a simplified system model.

Index	$\dot{V}_{S,P}$	$\dot{V}_{N_2, R}$
-	ml min^{-1}	ml min^{-1}
H1	7.2	3.4
H2	43.0	20.3
H3	46.9	22.2
H4	49.5	23.5
O1	4.1	3.0
O2	15.2	11.3
O3	15.9	11.9
O4	16.4	12.3

References

Campos-Martin, J., Blanco-Brieva, G., Fierro, J.G., 2006. Hydrogen Peroxide Synthesis: an Outlook Beyond the Anthraquinone Process. Angew. Chem. 45, 6962–6984. https://doi.org/10.1002/anie.200503779.

Centi, G., Perathoner, S., Abate, S., 2009. Direct Synthesis of Hydrogen Peroxide: Recent Advances: Design, Reactions and Characterization. In: Mizuno (Hg.) 2009 - Modern Heterogeneous Oxidation Catalysis, pp. 253–287. doi:10.1002/9783527627547.ch8.

Ciriminna, R., Albanese, L., Meneguzzo, F., Pagliaro, M., 2016. Hydrogen Peroxide: A Key Chemical for Today's Sustainable Development. ChemSusChem 9, 3374–3381. https://doi.org/10.1002/cssc.201600895.

Flaherty, D., 2018. Direct Synthesis of H2O2 from H2 and O2 on Pd Catalysts: Current Understanding, Outstanding Questions, and Research Needs. ACS Catal. 8, 1520–1527. https://doi.org/10.1021/acscatal.7b04107.

Fuller, E., Schettler, P., Giddings, J., 1966. New Method for Prediction of Binary Gas-Phase Diffusion Coefficients. Ind. Eng. Chem. 58, 18–27. https://doi.org/10.1021/ie50677a007.

García-Serna, J., Moreno, T., Biasi, P., Cocero, M.J., Mikkola, J.P., Salmi, T.O., 2014. Engineering in Direct Synthesis of Hydrogen Üeroxide: Targets, Reactors and Guidelines for Operational Conditions. Green Chem. 16, 2320. https://doi.org/10.1039/c3gc41600c.

Goor, G., Glenneberg, J., Jacobi, S., Dadabhoy, J., Candido, E., 2000. Hydrogen Peroxide. In: Ullmann's Encyclopedia of Industrial Chemistry. Wiley-VCH Verlag GmbH & Co. KGaA: Weinheim, Germany, pp. 1–40. doi:10.1002/14356007.a13_443.pub3.

Hägg, M., 2000. Membrane Purification of Cl2 gas I. Permeabilities as a Function of Temperature for Cl2,O2,N2,H2 in two Types of PDMS Membranes. J. Membr. Sci. 170, 173–190. https://doi.org/10.1016/S0376-7388(99)00371-3.

Li, J., Šimek, H., Ilioae, D., Jung, N., Bräse, S., Zappe, H., Dittmeyer, R., Ladewig, B.P., 2021. In Situ Sensors for Flow Reactors - a Review. Reaction Chem. Eng. https://doi.org/10.1039/D1RE00038A.

Merkel, T., Bondar, V., Nagai, K., Freeman, B., Pinnau, I., 2000. Gas Sorption, Diffusion, and Permeation in Polydimethylsiloxane. J. Polym. Sci., Part B: Polym. Phys. 38, 415–434. https://doi.org/10.1002/(SICI)1099-0488(20000201)38:3<415::AID-POLB8>3.0.CO;2-Z.

Nagy, E., 2012. Basic Equations of the Mass Transport Through a Membrane Layer. Elsevier Insights, Elsevier, Amsterdam and Boston.

Pashkova, A., Svajda, K., Dittmeyer, R., 2008. Direct Synthesis of Hydrogen Peroxide in a Catalytic Membrane Contactor. Chem. Eng. J. (Amsterdam, Neth.) 139, 165–171. https://doi.org/10.1016/j.cej.2007.09.003.

Pashkova, A., Dittmeyer, R., Kaltenborn, N., Richter, H., 2010. Experimental Study of Porous Tubular Catalytic Membranes for Direct Synthesis of Hydrogen Peroxide. Chem. Eng. J. (Amsterdam, Neth.) 165, 924–933. https://doi.org/10.1016/j.cej.2010.10.011.

Pashkova, A., Greiner, L., Krtschil, U., Hofmann, C., Zapf, R., 2013. Direct Synthesis of Hydrogen Peroxide Over Supported Pd Catalysts: Turning to Dense CO2 as an Alternative Solvent. Appl. Catal., A 464–465, 281–287. https://doi.org/10.1016/j.apcata.2013.06.007.

Paunovic, V., Schouten, J., Nijhuis, T.A., 2015. Direct Synthesis of Hydrogen Peroxide Using Concentrated H2 and O2 Mixtures in a Wall-Coated Microchannel – Kinetic Study. Appl. Catal., A 248, 160–168. https://doi.org/10.1016/j.cattod.2014.04.007.

Samanta, C., 2008. Direct Synthesis of Hydrogen Peroxide from Hydrogen and Oxygen: An Overview of Recent Developments in the Process. Appl. Catal., A 350, 133–149. https://doi.org/10.1016/j.apcata.2008.07.043.

Sander, R., 2015. Compilation of Henry's Law Constants (Version 4.0) for Water as Solvent. Atmos. Chem. Phys. 15, 4399–4981. https://doi.org/10.5194/acp-15-4399-2015.

Selinsek, M., Bohrer, M., Vankayala, B.K., Haas-Santo, K., Kraut, M., Dittmeyer, R., 2016. Towards a New Membrane Micro Reactor System for Direct Synthesis of Hydrogen Peroxide. Catal. Today 268, 85–94. https://doi.org/10.1016/j.cattod.2016.02.003.

Selinsek, M., Kraut, M., Dittmeyer, R., 2018. Experimental Evaluation of a Membrane Micro Channel Reactor for Liquid Phase Direct Synthesis of Hydrogen Peroxide in Continuous Flow Using Nafion Membranes for Safe Utilization of Undiluted Reactants. Catalysts 8, 556. https://doi.org/10.3390/catal8110556.

Shoghl, S., Raisi, A., Aroujalian, A., 2017. Modeling of Gas Solubility and Permeability in Glassy and Rubbery Membranes Using Lattice Fluid Theory. Polymer 115, 184–196. https://doi.org/10.1016/j.polymer.2017.03.032.

Urban, S., Weltin, A., Flamm, H., Kieninger, J., Deschner, B.J., Kraut, M., Dittmeyer, R., Urban, G.A., 2018. Electrochemical Multisensor System for Monitoring Hydrogen Peroxide, Hydrogen and Oxygen in Direct Synthesis Microreactors. Sens. Actuators, B 273, 973–982. https://doi.org/10.1016/j.snb.2018.07.014.

Urban, S., Tamilselvi Sundaram, V., Kieninger, J., Urban, G., Weltin, A., 2020. Microsensor Electrodes for 3D Inline Process Monitoring in Multiphase Microreactors. Sensors 20, 4876. https://doi.org/10.3390/s20174876.

Urban, S., Deschner, B.J., Trinkies, L.L., Kieninger, J., Kraut, M., Dittmeyer, R., Urban, G.A., Weltin, A., 2021. In Situ Mapping of H2, O2, and H2O2 in Microreactors: A Parallel, Selective Multianalyte Detection Method. ACS Sens. 6, 1583–1594. https://doi.org/10.1021/acssensors.0c02509.

VDI-Wärmeatlas: Mit 320 Tabellen, 11. ed.; VDI-Buch, Springer Vieweg and Springer, Berlin Heidelberg: Berlin, doi:10.1007/978-3-642-19981-3.

Wilson, N., Bregante, D., Priyadarshini, P., Flaherty, D., 2017. Production and Use of H2O2 for Atom-efficient Functionalization of Hydrocarbons and Small Molecules. Catal. 29, 122–212. https://doi.org/10.1039/9781788010634-00122.

Yampolskii, Y.P., Pinnau, I., Freeman, B.D., 2006. Materials Science of Membranes for Gas and Vapor Separation. Wiley, Chichester England and Hoboken NJ.

Yang, S., Verdaguer-Casadevall, A., Arnarson, L., Silvioli, L., Colic, V., 2018. Toward the Decentralized Electrochemical Production of H2O2: A Focus on the Catalysis. ACS Catal. 8, 4064–4081. https://doi.org/10.1021/acscatal.8b00217.

Yi, Y., Wang, L., Li, G., Guo, H., 2016. A Review on Research Progress in the Direct Synthesis of Hydrogen Peroxide from Hydrogen and Oxygen: Noble-Metal Catalytic Method, Fuel-Cell Method and Plasma Method. Catal Sci. Technol. 6, 1593–1610. https://doi.org/10.1039/C5CY01567G.